Explainable PET-Based Habitat and Peritumoral Machine Learning Model for Predicting Progression-free Survival in Clinical Stage IA Pure-Solid Non-small Cell Lung Cancer: A Two-center Study

Bei-Hui Xue, Shuang-Li Chen, Jun-Ping Lan, Li-Li Wang, Jia-Geng Xie, Xiang-wu Zheng, Liang-Xing Wang[1], Kun Tang[1]

Rationale and Objectives: This study aimed to develop and validate machine learning (ML) models utilizing positron emission tomography (PET)-habitat of the tumor and its peritumoral microenvironment to predict progression-free survival (PFS) in patients with clinical stage IA pure-solid non-small cell lung cancer (NSCLC).

Materials and Methods: 234 Patients who underwent lung resection for NSCLC from two hospitals were reviewed. Radiomic features were extracted from both intratumoral, peritumoral and habitat regions on PET. Univariate and multivariate logistic regression analyses were employed to determine significant clinical variables. Subsequently, a radiomics nomogram was developed by combining the radiomics signature with these identified clinical variables. Kaplan–Meier (KM) analysis was performed to investigate the prognostic value of the nomogram. Shapley Additive Explanations (SHAP) were used to interpret the ML models.

Results: The combination model which contained peritumoral 5 mm and habitat regions radiomics features, clinical variables obtained a strong well-performance, achieving area under the curve (AUC) of 0.905 (95% confidence interval (CI) 0.854–0.957) in the train set and 0.875 (95% CI 0.789–0.962) in the internal validation set. The radiomics signature was significantly associated with PFS, the model significantly discerned high and low-risk patients, and exhibited a significant benefit in the clinical use showed low-risk score given have far longer RFS than those with high-risk score (log-rank P < 0.001).

Conclusion: The habitat and peritumoral radiomics signatures serve as an independent biomarker for predicting PFS in patients with early-stage NSCLC, effectively stratified survival risk among patients with clinical stage IA pure-solid non-small cell lung cancer.

Key Words: Lung cancer; Radiomics; ^{18}F-FDG PET; Neoplasm recurrence.

Abbreviations: **PFS** Progression-free survival, **NSCLC** Non-small cell lung cancer, **AUC** Area under the curve, **DCA** Decision curve analysis, **KM** KaplaneMeier, **SHAP** Shapley Additive Explanations, **ML** Machine learning, **CTR** Consolidation tumor ratio, **ROI** Regions of interest, **VOI** Volume of Interest, **LASSO** Least absolute shrinkage and selection operator, **LightGBM** Light gradient boosting machine, **OR** Odds ratio, **CI** Confidence interval, **ROC** Receiver operating characteristic, **GLCM** Gray-level co-occurrence matrix, **GLSZM** Gray-level size zone matrix, **GLRLM** Gray-level run length matrix, **NGTDM** Neighboring gray tone difference matrix, **GLDM**

Acad Radiol 2025; 32:3687–3698

From the Division of Pulmonary Medicine, the First Affiliated Hospital of Wenzhou Medical University, Key Laboratory of Heart and Lung, Wenzhou, Zhejiang, China (B.H.X., J.P.L.); Department of Radiology, The First Affiliated Hospital of Wenzhou Medical University, Wenzhou, China (B.H.X., S.L.C., J.G.X., X.W.Z.); Department of Nuclear Medicine, The First Affiliated Hospital of Wenzhou Medical University, Wenzhou, Key Laboratory of Novel Nuclide Technologies on Precision Diagnosis and Treatment & Clinical Transformation of Wenzhou City, China (K.T.); Division of Pulmonary Medicine, The First Affiliated Hospital of Wenzhou Medical University, Wenzhou Key Laboratory of Interdiscipline and Translational Medicine, Wenzhou Key Laboratory of Heart and Lung, Wenzhou, China (L.X.W.); Department of Radiology, Wenzhou Central Hospital, China (L.L.W.). Received November 23, 2024; revised December 17, 2024; accepted December 17, 2024. **Address correspondence to:** K.T. e-mail: kuntang007@wmu.edu.cn

[1] Kun Tang, Liang-Xing Wang contributed equally to this work.

https://doi.org/10.1016/j.acra.2024.12.038

Gray-level dependence matrix, **SUVmax** Maximum standardized uptake value, **CEA** Carcinoembryonic antigen, **SCCA** Squamous cell carcinoma antigen, **NSE** Neuron-specific enolase, **CYFRA21–1** Cytokeratin 19 fragment, **ALB** Albumin, **WBC** White blood cell, **MONO** Monocyte, **Lym** Lymphocyte, **Neu** Neutrophil

INTRODUCTION

Lung cancer is the leading cause of cancer-related deaths globally and is expected to account for about 21% of all cancer deaths in 2023 (1). Among them, lung adenocarcinoma is the most common subtype of lung cancer, accounting for about 50% of all lung cancer cases. (2). With the rapid advancement of computed tomography (CT) screening technology, an increasing number of non-small cell lung cancer (NSCLC) cases are being diagnosed in the early stage, especially those in clinical stage IA with tumors diameter less than 3 cm (3). Pulmonary nodules are categorized according to the CT consolidation tumor ratio $(CTR)^2$ into subsolid nodules ($0 \leq CTR < 1$) and pure-solid nodules ($CTR = 1$) (4). Previous studies have demonstrated that pure-solid nodules, even after standard surgical procedures, tent to exhibit more aggressive malignant behavior and are associated with poorer prognoses compared to subsolid nodules and pure ground-glass opacity nodules (5,6). Although stage IA pure solid nodules have a relatively better prognosis compared to other stages, patients still exhibit diverse prognosis following surgical resection, and may require different treatment approaches (7,8). Therefore, constructing more effective prognostic tools tailored specifically for clinical stage IA pure-solid NSCLC is warranted.

Advancements in biologic and genomic technologies have significantly improved survival estimation by enabling the integration of survival-associated biologic and genetic signatures (9,10). However, a limitation of these invasive methods is their inability to capture comprehensive information about heterogeneous tumors. The radiomics approach involves transforming medical images into quantitative data to aid in noninvasive clinical decision-making (11). Habitat imaging is an innovative technique for tumor characterization, which involves segmenting tumors into various subregions for more detailed analysis, provides a more precise quantification of heterogeneity within tumors (12,13). The peritumoral region of a lesion may possess characteristics related to the tumor microenvironment, which could be important for enhancing tumor diagnosis and predicting prognosis. Traditional machine learning models often suffer from a lack of interpretability, resulting in the "black box" problem, which poses challenges for clinical application. The Shapley Additive Explanations (SHAP) method addresses this issue by providing interpretability through both global and local explanations, helping to clarify the decision-making processes of these models (14,15).

We hypothesized that integrating radiomic features from both the habitat and peritumoral regions could improve the accuracy of prognosis prediction for pure-solid NSCLC. Therefore, this study aimed to develop and validate a radiomics signature that utilizes multidimensional features for personalized survival risk stratification in patients with stage IA pure-solid NSCLC.

METHODS

Patient Cohorts

A total of 234 consecutive patients who underwent lung resection confirmed with clinical stage IA pure-solid NSCLC were screened in two independent institutions. The inclusion criteria were as follows: (I) preoperative PET-CT was performed; (II) complete clinical and pathological data; (III) clinical stage IA NSCLC (cT1N0M0); (IV) the interval less than 30 days between PET-CT examination and surgery; (V) pure solid nodules; The exclusion criteria were as follows: (I) poor image quality; (II) lost to follow-up; (III) preoperative neoadjuvant and chemotherapy; (IV) biopsy and tissue sampling before PET-CT examination. This study was approved by the institutional ethics review boards and was conducted in accordance with the principles outlined in the Declaration of Helsinki. Since this was a retrospective study, informed consent was not required. Patients from two centers were randomly assigned into the training and internal validation cohorts at a ratio of 7:3. A flowchart of patient selection is shown Figure 1.

Data Collection

Among all the patients, their clinical data (age, sex, smoking history); PET metabolic parameters (maximum standardized uptake value (SUVmax)); CT imaging features (lobulation, spiculation, air-bronchogram, vascular-convergence, pleural retraction, tumor location) and blood markers (carcinoembryonic antigen (CEA), squamous cell carcinoma antigen (SCCA), neuron-specific enolase (NSE), cytokeratin 19 fragment (CYFRA21–1), albumin (ALB), white blood cell (WBC), monocyte (MONO), lymphocyte (Lym),neutrophil (Neu)) were recorded.

Follow-up Surveillance

Patients are required to follow-up via chest CT scans every 6–12 months for the first two years, and subsequently once every 12 months thereafter. Disease recurrence was diagnosed based on suspicious radiologic findings or histologically confirmed disease. The target variable of this study was PFS, defined as the period from the PET/CT examination date to either the relapse date (event)—encompassing tumor recurrence within or adjacent to the treated area, mediastinal relapse, distant relapse, or death—or the last date the patient was confirmed to be relapse-free (censored), and the last

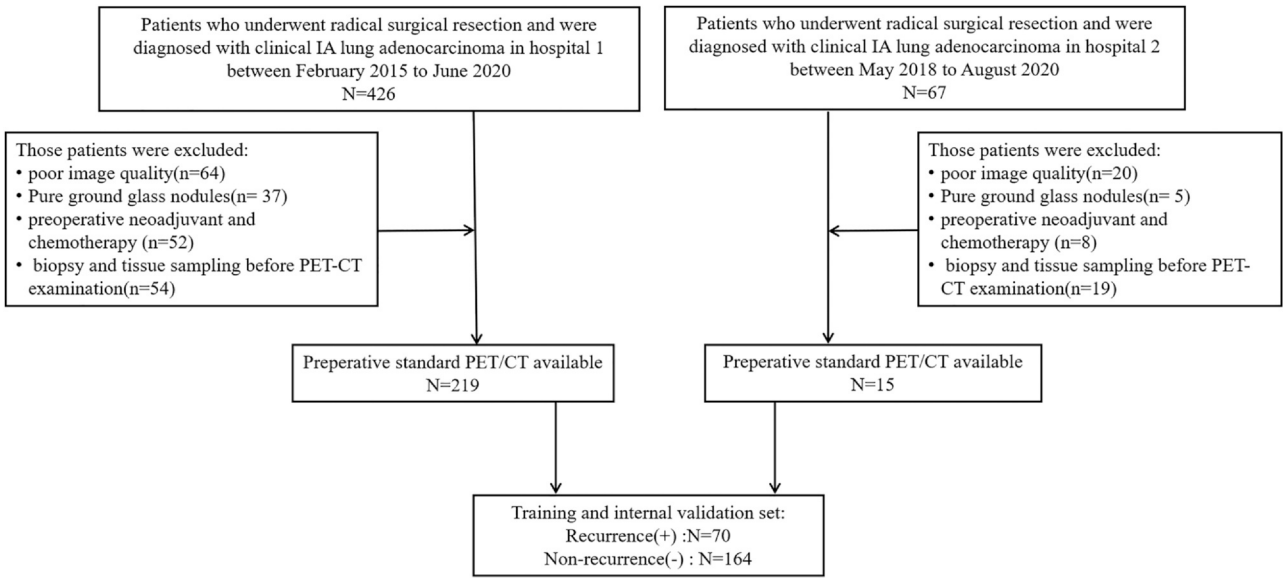

Figure 1. Proceeding flow of enrollment.

follow-up occurred in June 2024. The minimum follow-up duration to ascertain PFS was set at 48 months following the initial CT study, with the maximum follow-up extending to 113 months.

The optimal cutoff value for the signature was determined using the X-tile program based on its association with survival outcomes (16). Patients were then classified into low- and high-risk groups, and their survival outcomes were compared using Kaplan–Meier analysis and log-rank tests. Multivariable analyses were conducted to identify independent prognostic risk factors.

PET/CT Image Acquisition

The patients received an intravenous injection of ^{18}F-FDG (3.7 MBq/kg) after fasting for at least 6 h. Blood glucose level was maintained below ML/dl. Approximately 60 min later, images were acquired using a hybrid PET/CT scanner (GEMINI TF 64, Philips, Netherlands). A low dose, unenhanced CT scan, spanning from the skull base to the middle of the thighs, was conducted using specific parameters: 120 kV, 80 mA, pitch of 0.829, and reconstruction thickness and interval of 5.0 mm. Subsequently, a 3D model was utilized to generate PET images. The imaging parameters included a field of view of 576 mm, a matrix size of 144 × 144, slice thickness and interval of 5 mm, and an emission scan time of 1.5 min for each bed position. PET images with CT attenuation correction were reconstructed using the time-of-flight algorithm.

Image Segmentation and Preprocessing

The workflow of radiomics is shown in Figure 2. In order to enhance the robustness of radiomic features and ensure their suitability for further analysis, image preprocessing was conducted prior to segmentation and feature extraction, addressing the variations of PET/CT scans used in this study. Image preprocessing involved isotropic spatial resampling, where 2 mm spatial resampling had a smaller impact on the calculation of radiomic features compared to 1 mm and 4 mm resampling (17). All patients' PET images were resampled to 2 mm in the X, Y, and Z directions. Intensity discretization and rescaling were automatically performed by the software. The regions of interest (ROI) were segmented using LIFEx (18) software (https://www.lifexsoft.org/). Based on the metabolic threshold of PET images, we were able to rapidly delineate the tumor contour.

The region of interest for the tumor was semi-automatically delineated layer by layer by using 3D plotting tools without prior knowledge of the patient's clinical data and mutational status. To evaluate the robustness of the segmentation process, 50 patients were randomly selected for segmentation by two radiologists.

Peritumoral Regions Dilation and Habitat Generation

After segmentation, peritumoral masks were created using morphologic dilation. Various peritumoral regions were examined by setting dilation intervals of 1 mm, 3 mm, and 5 mm to evaluate their effects on the model's predictive performance, including PERI1mm, PERI3mm, and PERI5mm. Bronchi, large vessels, and normal tissue were manually excluded. Local features, including local entropy and energy values, were extracted by analyzing each voxel within the specified volume of interest (VOI). These features were then clustered into subregions using the K-means method, resulting in the formation of multiple distinct habitats. The number of habitats tested ranged from 2 to 10, and the optimal k-value was determined using the Consensus Cluster method. The process of habitat generation and the specific features are illustrated in Figure 3.

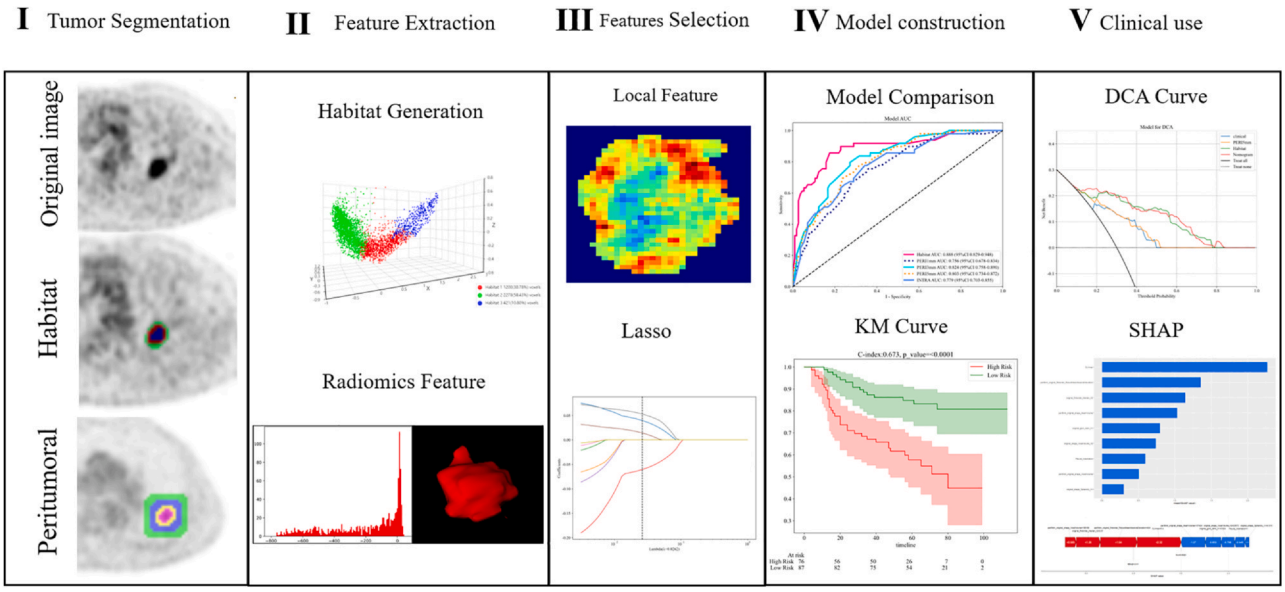

Figure 2. Workflow of necessary steps on PET images.

Feature Extraction and Selection

All features were extracted with the Pyradiomics tool. The extracted radiomic features were divided into seven categories: shape features, first-order statistics, Gray-level co-occurrence matrix (GLCM) features, Gray-level size zone matrix (GLSZM) features, Gray-level run length matrix (GLRLM) features, neighboring gray tone difference matrix (NGTDM) features, and Gray-level dependence matrix (GLDM) features.

Intraclass correlation coefficients were calculated for lesions segmented by multiple radiologists. For feature selection, the imaging features were standardized using Z-score normalization to adjust the data to a mean of zero and a variance of one. When the correlation between features exceeded the threshold of 0.9, only one feature from each highly correlated pair was retained to eliminate redundancy. Finally, a two-sample T-test and the least absolute shrinkage and selection operator (LASSO) regression model were applied to further refine the selected features in the training dataset.

Development and Validation of Machine Learning Models

Among the range of machine learning models, we selected light gradient boosting machine (LightGBM) construct radiomics signatures for intratumoral, peritumoral, and habitat regions, derived from the final feature set. It utilizes an innovative technique known as histogram-based binning, allowing for more efficient learning compared to other algorithms. While tree-based models like XGBoost construct trees using a level-wise growth approach, LightGBM adopts a leaf-wise growth strategy instead of the traditional level-wise method to build its trees (19). The SHAP explanation was used to measure each feature's importance to the machine learning model. The SHAP value's magnitude indicates its contribution to the prediction, and its sign denotes whether the effect is positive or negative.

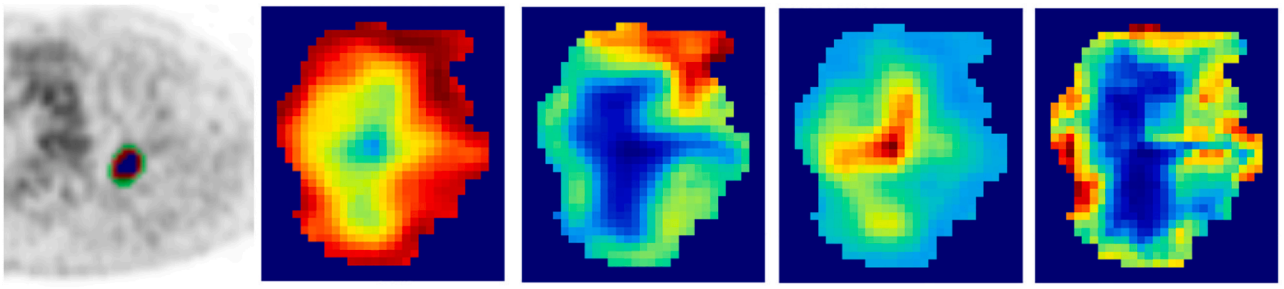

Figure 3. The generated habitat regions and specific characteristics are presented.

Statistical Analyses

Data analyses were performed using Python (version 3.7.3, https://www.python.org), R (version 4.3.0, https://www.r-project.org), and SPSS Statistical (Version 22.0, https://www.ibm.com/spss) Software. Continuous numerical variables were compared using the Mann–Whitney U test or t test. Categorical data were evaluated using chi-square tests or Fisher's exact tests to assess difference between groups. The clinical factors that showed statistical significance in the univariable analysis were included in a multivariable logistic regression to ascertain independent predictors with odds ratio (OR) and 95% confidence interval (CI). Receiver operating characteristic (ROC) curves were plotted, and the area under the curve (AUC), accuracy, sensitivity, and specificity were calculated to evaluate the predictive performance of different models. The net benefit of the predictive models assessed by decision curve analysis (DCA). A two-tailed P value < 0.05 was considered statistically significant.

RESULTS

Patient Characteristics

Patients were divided into two groups based on the presence or absence of recurrence. The clinicalpathologic characteristics are shown in detail in Table 1. In our study, the rates of recurrence were found to be 30.06% and 29.58% in the training and validation sets, respectively. Univariate and multifactorial analyses of clinical features were performed with OR and corresponding P-values calculated for each feature (Table 2). Univariate analysis revealed that sex, air bronchogram, lobulation, spiculation, smoking, pleural indentation, differentiation, tumor location and SUVmax value were significantly different between the recurrence and non-recurrence groups. Multivariate analysis revealed that pleural indentation (OR, 1.892; 95% CI, 1.137–3.152; P = 0.040) and SUVmax(OR, 1.203; 95% CI, 1.016–1.423; P = 0.021) were independently correlated with the recurrence status.

Radiomics Feature Selection and Optimal Signature Construction

A total of 107 handcrafted radiomic features were extracted across various subsets, features with an intraclass correlation coefficient $<$ 0.8 or exhibiting minimal variance were excluded to ensure stability and reproducibility, subsequently refined using the Lasso method. The optimal k-value, which was found to be 3, used as the criterion for determining the ideal number of clusters at the population level. Lung cancer tumors were classified into three distinct categories: habitat 1, habitat 2, and habitat 3. The optimal λ values for PERI1mm, PERI3mm, and PERI5mm and habitat were 0.0339, 0.0010, 0.0168, and 0.0262, respectively. These optimal λ values resulted in 3, 5, 3, and 4 selected features for constructing four radiomics models. After obtaining the optimal features, we proceeded to build and compare the performances of these different models.

Performance of Different Models

In the train set, several signatures showed strong AUC values, with the highest AUC observed for the habitat signature of 0.888 (95% CI: 0.829–0.948). The AUC values for three different settings in the peritumoral regions were PERI1mm 0.756 (95% CI: 0.678–0.834), PERI3mm 0.824 (95% CI: 0.758–0.890), and PERI5mm 0.803 (95% CI: 0.734–0.872), respectively, while the AUC for Intra was 0.779 (95% CI: 0.703–0.855). In the validation set, the habitat signature achieved the highest AUC, with a value of 0.828 (95% CI: 0.729–0.926). The AUC value of the PERI5mm signature was 0.827 (95% CI: 0.710–0.943), which outperformed the other three radiomic signatures (Intra, 0.754; PERI1mm, 0.788; PERI3mm, 0.680). The accuracy, sensitivity, specificity, negative predictive value, and positive predictive value are listed in Table 3. Selecting the peritumoral model with the highest AUC on the test set. SUVmax and pleural indentation were identified as an independent factor associated with recurrence and were integrated with representative signatures (PERI5mm, habitat) to create a nomogram, with a value of 0.905 (95% CI: 0.854–0.957) in the train set and 0.875 (95% CI: 0.789–0.962) in the validation set (Fig 4). The DCA of different models in training and validation sets showed that nomogram provided a better net benefit than other radiomics models for the most of the threshold range (Fig 5).

Survival Risk Stratification Based on the Radiomics Signature and Model Interpretation

All patients with pure-solid tumors were divided into low-risk and high-risk groups based on the optimal cutoff value (radiomics score, 0.55) of the radiomics signature determined by X-tile. The analysis of the radiomics signature revealed that patients with lower scores tended to have better PFS, while those with higher scores were associated with an increased risk of recurrence. The radiomics signature showed a significant association with PFS (P = $<$0.0001) in the training set. This result was further validated in the validation set, where the radiomics signature remained significantly also associated with PFS (P = $<$ 0.0001). (Fig 6).

We calculated both the overall and individual Shapley values to interpret the combined model and support its clinical application. In the overall visualization, the SHAP bar chart (Fig 7a) shows the weights of the different characteristics (radiomics features, SUVmax, Pleural_indentation) of the model. The SUVmax value showed the highest weight. The SHAP bees-warm plot (Fig 7b) illustrates the positive and negative impacts of each feature on the prediction probability, represented by yellow and purple, respectively. The SHAP effort plot (Fig 7c/d) shows each feature's positive and negative effects on predictive outcomes

TABLE 1. Characteristics of Non-small Cell Lung Cancer Patients in the Training and Validation Cohorts

	Train set (*n* = 163)			Validation set (*n* = 71)		
Characteristic	non-recurrence (*n* = 114)	recurrence (*n* = 49)	P	non-recurrence (*n* = 50)	recurrence (*n* = 21)	P
Mean age (y)	63.43 ± 9.46	64.31 ± 11.16	0.548	61.36 ± 9.71	63.67 ± 10.24	0.371
Sex			0.505			0.725
Male	57(50.00%)	28(57.14%)		23(46.00%)	8(38.10%)	
Female	57(50.00%)	21(42.86%)		27(54.00%)	13(61.90%)	
Smoking history			0.437			0.498
Ever	83(72.81%)	32(65.31%)		41(82.00%)	15(71.43%)	
Never	31(27.19%)	17(34.69%)		9(18.00%)	6(28.57%)	
CEA(μg/L)			0.388			0.261
≤ 5	89 (78.07%)	36 (88.70%)		41 (82.00%)	16 (76.19%)	
> 5	25 (21.93%)	13 (11.30%)		9 (18.00%)	5 (23.81%)	
SCCA (μg/L)	0.70 [0.60, 1.00]	0.80[0.60,1.00]	0.744	0.96[0.67,1.53]	1.22[0.82,1.53]	0.458
CYFRA21−1	2.14[1.05, 2.95]	2.96[2.19,3.12]	0.044	1.92[1.39, 2.82]	2.10[1.45,2.90]	0.484
NSE (ng/ML)	14.20[11.55,16.45]	14.20[11.95,16.35]	0.829	14.50[11.60,16.95]	15.85[13.68,16.90]	0.293
ALB	41.80 ± 4.35	42.60 ± 5.82	0.031	40.23 ± 4.06	36.94 ± 5.94	0.121
WBC	6.10[5.01,7.51]	6.41[5.28,7.82]	0.153	6.30[4.85,7.55]	5.65[4.70,6.92]	0.335
MONO	0.38[0.29,0.47]	0.38[0.28,0.51]	0.634	0.45[0.36,0.56]	0.37[0.35,0.48]	0.408
Lym	1.76[1.32,2.14]	1.74[1.33,2.19]	0.797	1.701.45,1.95]	1.45[1.30,1.60]	0.128
Neu	3.70[2.76,4.74]	4.13[3.16,4.85]	0.088	3.80[2.80,4.80]	3.15[2.90,4.40]	0.603
Tumor Location			0.503			0.833
Right upper lobe	36(31.58%)	13(26.53%)		14(28.00%)	6(28.57%)	
Right middle lobe	6(5.26%)	8(16.33%)		6(12.00%)	4(19.05%)	
Right lower lobe	25(21.93%)	8(16.33%)		14(28.00%)	1(4.76%)	
Left upper lobe	29 (25.44%)	16(32.65%)		11(22.00%)	8(38.10%)	
Left lower lobe	18(15.79%)	4(8.16%)		5(10.00%)	2(9.52%)	
Lobulation			0.771			0.200
No	58(50.88%)	23(46.94%)		19(38.00%)	4(19.05%)	
Yes	56(49.12%)	26(53.06%)		31(62.00%)	17(80.95%)	
Differentiation			< 0.001			0.188
Well-differentiated	10(8.77%)	6(12.25%)		3(6.00%)	1 (4.76%)	
Moderately differentiated	90(78.95%)	25(51.02%)		43(86.00%)	15(71.43%)	
Poorly differentiated	14(12.28%)	18(36.73%)		4(8.00%)	5(23.81%)	
Spiculation			0.382			0.576
No	75(65.79%)	28(57.14%)		36(72.00%)	13(61.90%)	
Yes	39(34.21%)	21(42.86%)		14(28.00%)	8(38.10%)	
Air-bronchogram			0.726			0.899
No	95(83.33%)	39(79.59%)		43(86.00%)	19(90.48%)	
Yes	19(16.67%)	10(20.41%)		7(14.00%)	2(9.52%)	

Table 1 (*Continued*)

	Train set (*n* = 163)			Validation set (*n* = 71)		
Characteristic	non-recurrence (*n* = 114)	recurrence (*n* = 49)	P	non-recurrence (*n* = 50)	recurrence (*n* = 21)	P
Vascular-convergence			1.000			0.370
No	92(80.70%)	39(79.59%)		44(88.00%)	16(76.19%)	
Yes	22(19.30%)	10(20.41%)		6(12.00%)	5(23.81%)	
Pleural retraction			0.175			0.075
No	66(57.89%)	22(44.90%)		25(50.00%)	5(23.81%)	
Yes	48(42.11%)	27(55.10%)		25(50.00%)	16(76.19%)	
SUVmax	4.66[2.80, 6.20]	6.42 [4.21, 8.65]	< 0.001	2.95 [1.60, 5.32]	7.19 [5.11, 10.54]	0.004
Recurrence-free time (mo)	69.05[56.00, 80.25]	28.45[13.00, 39.75]	< 0.001	68.66[54.00, 81.75]	29.24[19.00, 39.50]	< 0.001

ALB, albumin; CEA, carcinoembryonic antigen; CYFRA21-1, cytokeratin 19 fragment; Lym, lymphocyte; MONO, monocyte; Neu, neutrophil; NSE, neuron-specific enolase; SUVmax, maximum standardized uptake value; SCCA, squamous cell carcinoma antigen; WBC, white blood cell

in a single case. The features in red increase output while the features in blue do the opposite.

DISCUSSION

The PET-radiomics based model for the estimation of PFS in patients with clinical stage IA pure-solid NSCLC, particularly through habitat and peritumoral regions analysis, enhances our understanding of tumor heterogeneity and improves the prediction of survival outcomes. Notably, the radiomics nomogram outperformed traditional clinical factors, could therefore allow risk stratification of patients highlighting its enhanced utility in providing individualized PFS predictions for early-stage NSCLC patients.

In recent years, ^{18}F-FDG PET/CT scan which simultaneously offers both anatomical and metabolic insights into tumors, has garnered significant interest in the evaluation of NSCLC and other lung lesions (20,21). There is significant variability in the prognoses of patients with NSCLC, emphasizing the importance of precise survival risk stratification for effective treatment planning (22). The identified signature consisted of the following features: original_glcm_ldmn_h1, original_firstorder_Median_h2,Peri5mm_original_firstorder_RobustMeanAbsoluteDeviation,Peri5mm_original_shape_MeshVolume,original_shape_VoxelVolume_h2, Peri5mm_original_shape_VoxelVolume and original_shape_Sphericity_h1, which are similar to the results of recent studies of risk stratification (23,24).

Radiomics, a high-throughput quantitative analysis technique, demonstrates significant potential in the field of NSCLC (25). Increasing studies have shown that habitat radiomics could be used to develop diagnostic or prognostic cancer biomarkers. Zhang et al. (26) reported that habitat imaging allows for the quantification and visualization of various subregions within the tumor, which noninvasively and preoperatively determined the microvascular invasion of hepatocellular carcinoma with high accuracy. Wu et al. (27) demonstrated that habitat radiomic features exhibited superior predictive ability compared to other individual models, showing promising performance in distinguishing between EGFR mutant and wild-type cases. Our results also underscored the significance of habitat imaging, as it achieved the highest AUC value among the different models. It is important to note that habitat radiomics combines the benefits of conventional radiomics with the analysis of intratumoral spatial heterogeneity. And the habitat which identified through PET imaging tend to be more heterogeneous and eccentric, often correlating with a poorer prognosis. However, these studies primarily concentrated on features that describe the heterogeneity of the tumor's core area, overlooking the predictive value of imaging information obtained from the peritumoral region. Tumor invasion into the peripheral region affects the survival outcomes of cancer patients and may be indicated by morphologic changes. Numerous studies highlight the importance of

TABLE 2. Univariable and Multivariable Logistic Regression Analysis of Factors in the Training Cohort

characteristic	Univariate logistic		Multivariate logistic	
	Odds Ratio (95%CI)	P	Odds Ratio (95%CI)	P
Sex	0.405 (0.290–0.566)	< 0.001	0.943 (0.519–1.713)	0.871
Air-bronchogram	0.462 (0.260–0.820)	0.027	0.875 (0.446–1.719)	0.745
Lobulation	0.494 (0.364–0.672)	< 0.001	1.147 (0.686–1.917)	0.661
Spiculation	0.547 (0.374–0.800)	0.009	1.143 (0.664–1.970)	0.686
Smoking	0.575 (0.374–0.884)	0.034	1.296 (0.668–2.512)	0.519
Pleural_indentation	0.589 (0.430–0.808)	0.006	1.892 (1.137–3.152)	0.040
Differentiation	0.708 (0.635–0.789)	< 0.001	1.257 (0.824–1.917)	0.374
Tumor Location	0.799 (0.742–0.862)	< 0.001	0.492 (0.828–1.142)	0.774
SUVmax	0.936 (0.901–0.972)	< 0.001	1.203 (1.016–1.423)	0.021

CI, confidence interval; SUVmax, maximum standardized uptake value

TABLE 3. Prediction Performance of Radiomics Models in Training Set and Validation Set

Signature	Accuracy	AUC	95%CI	Sensitivity	Specificity	Precision	F1	Cohort
Habitat	0.828	0.888	0.829–0.947	0.828	0.842	0.684	0.736	Train
PERI1mm	0.675	0.756	0.678–0.834	0.735	0.649	0.474	0.576	Train
PERI3mm	0.742	0.824	0.758–0.889	0.776	0.728	0.551	0.644	Train
PERI5mm	0.718	0.803	0.733–0.871	0.735	0.711	0.522	0.610	Train
INTRA	0.706	0.779	0.702–0.854	0.694	0.711	0.507	0.586	Train
Habitat	0.789	0.828	0.729–0.926	0.619	0.860	0.650	0.634	Test
PERI1mm	0.718	0.788	0.673–0.903	0.857	0.660	0.514	0.643	Test
PERI3mm	0.620	0.680	0.541–0.817	0.524	0.660	0.393	0.449	Test
PERI5mm	0.817	0.827	0.709–0.943	0.619	0.900	0.722	0.667	Test
INTRA	0.732	0.754	0.626–0.880	0.762	0.720	0.533	0.627	Test

AUC, area under the curve; CI, confidence interval

utilizing radiomics techniques to capture information about the surrounding regions of tumors (28,29). Shang et al (30) have demonstrated that derived from tumoral and peritumoral habitat imaging could help predict lung adenocarcinoma invasiveness. We have used radiomic features to find that the peritumoral regions have a potential predictive ability for the prediction of the recurrence status, with the PERI5mm signature having the best performance.

Unlike previous prognostic studies, which predominantly analyzed patients across all stages of the disease, our current

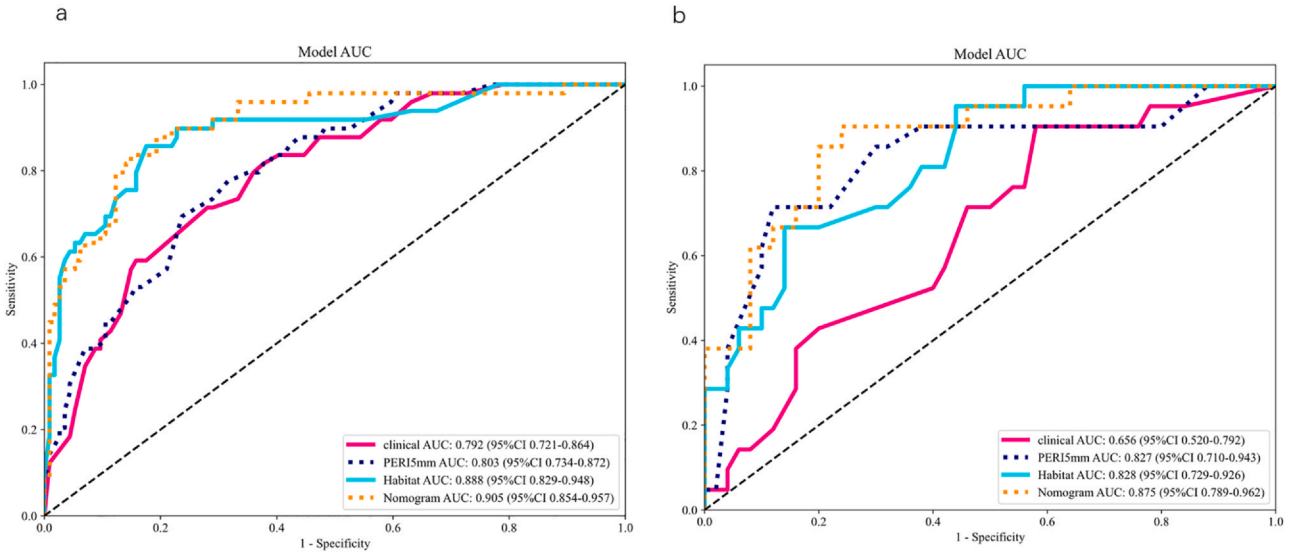

Figure 4. The ROC curves of the different models in the training set **(a)** and validation set **(b)**.

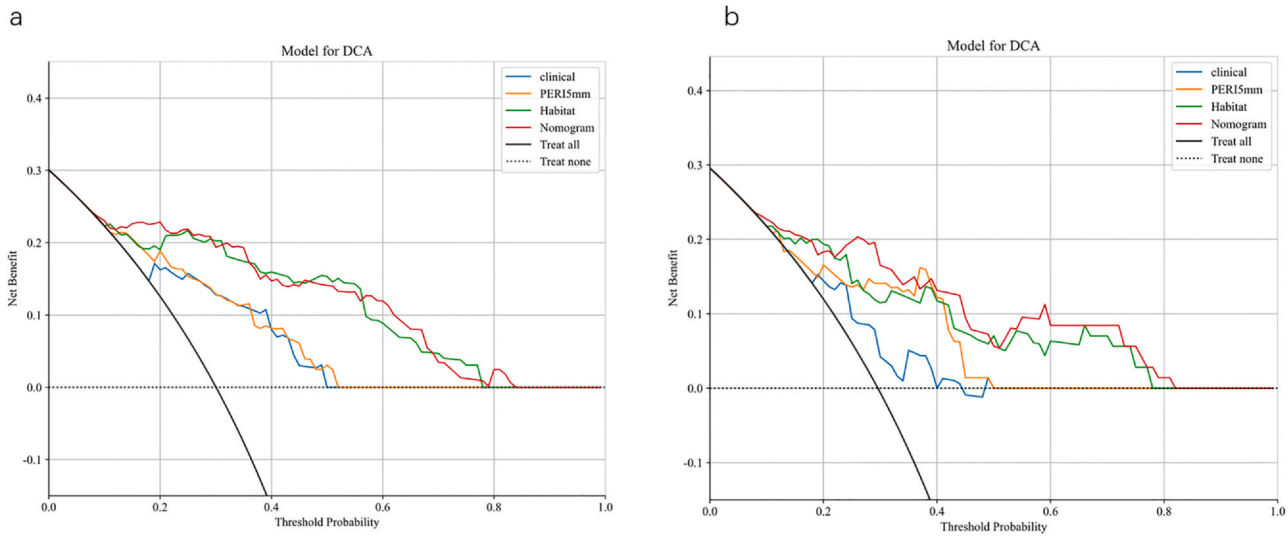

Figure 5. The decision curve analysis for the different models in training **(a)** and validation **(b)** sets showed that nomogram provided a better net benefit than other radiomics models for the most of the threshold range.

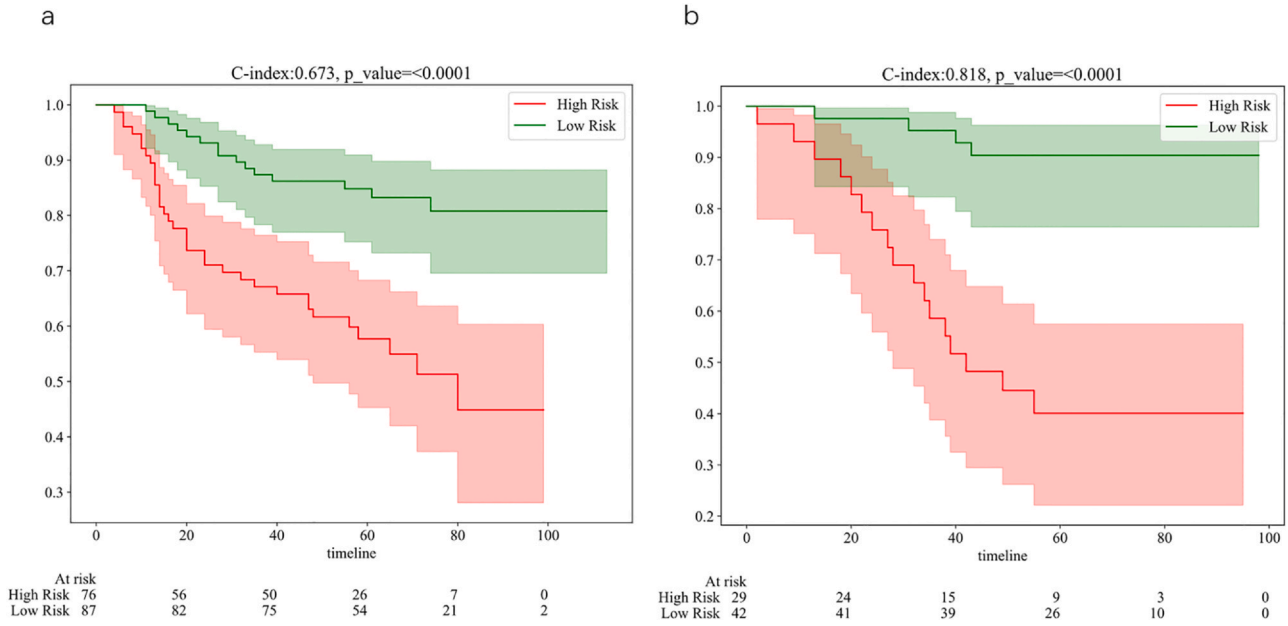

Figure 6. The KM survival curves of recurrence-free survival in patients between the two groups separated by low- and high-risk groups in training **(a)** and validation **(b)** sets.

research specifically focuses on patients with early-stage disease. It is important to note that survival outcomes showed variability, even among patients classified within the same clinical stage. In addition, several of earlier studies have demonstrated that clinical stage IA NSCLC with a pure-solid appearance exhibits relatively invasive oncological characteristics (31–33). Therefore, conducting a separate radiomic analysis specifically for clinical stage IA pure-solid NSCLC is both essential and warranted. The radiomics signature successfully stratified patients into high-risk and low-risk groups, identifying those who may benefit from more intensive treatment approaches. Moreover, the prognostic significance of clinical features is undeniable. Our efforts to integrate multidimensional and multiregional data highlights the significance of intratumor heterogeneity, the surrounding tumor microenvironment and clinical status in patient stratification.

The primary challenge in the field of radiomics currently lies in the interpretability of radiomic features. This study utilized SHAP analysis to demonstrate the contribution of each feature to the model's performance. SHAP is a widely used machine learning technique for gaining insights into the complex relationships between features and model predictions (34). The SHAP bar chart indicated SUVmax was

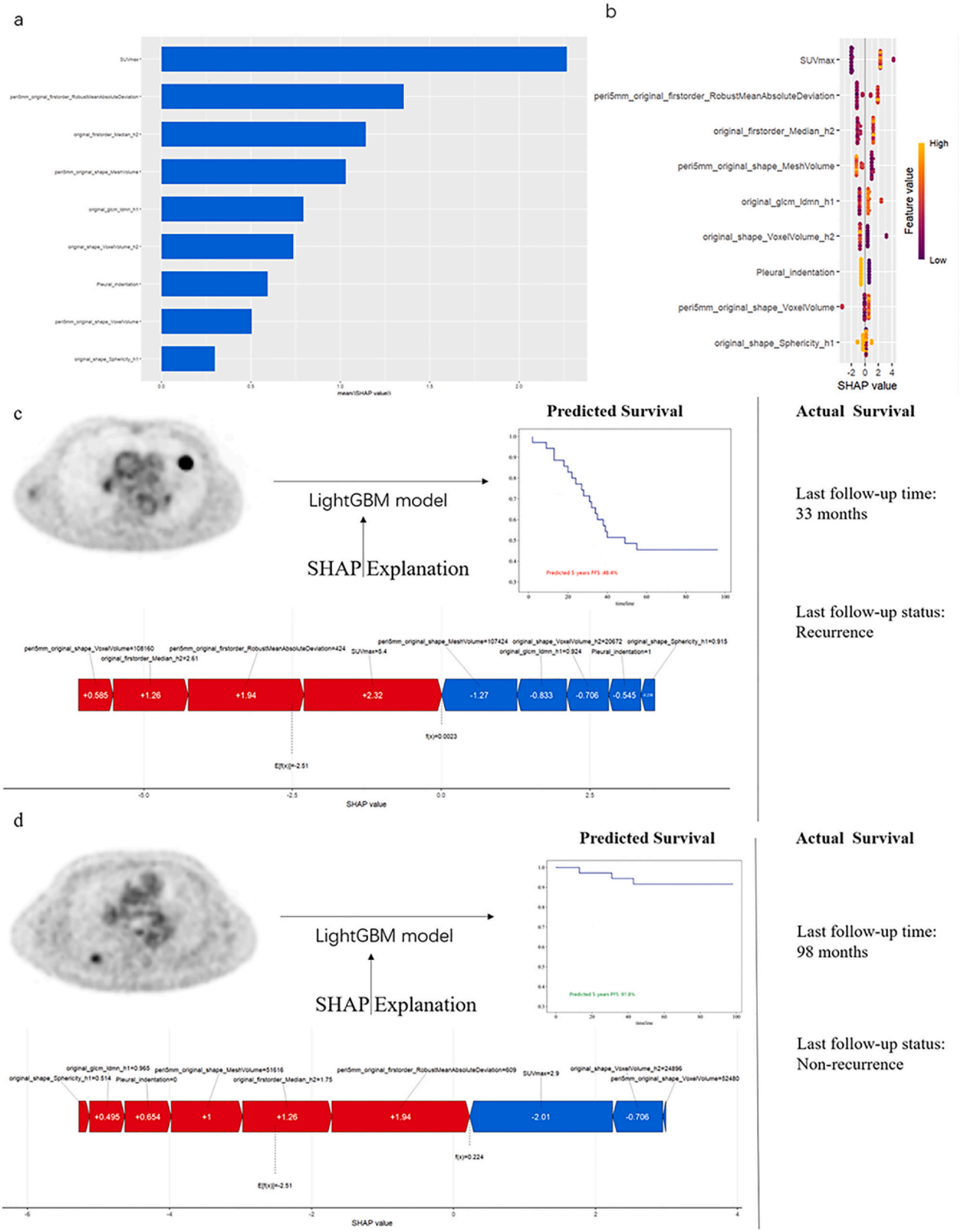

Figure 7. Overall visualization of the model through SHAP. The SHAP bar chart shows the weight of the different characteristics in the model **(a)**. The SHAP bees-warm plot shows the positive or negative effects of each feature on the prediction probability through yellow and purple colors **(b)**. The SHAP force plot shows the impact process of each significant features on the final predicted probability. A 75-year-old male with clinical stage IA3 NSCLC has a lower predicted 5-year survival of 48.4%, matched by actual survival at 33 months **(c)**. A 48-year-old female with clinical IA2 NSCLC shows a high predicted 5-year survival of 91.8%, with actual survival more than 98 months **(d)**.(Color version of figure is available online.)

identified as the most important feature of the model, this finding is consistent with current studies (35,36), SUVmax was the most significant predictor of local recurrence. In two examples, the SHAP explanation clearly showed the contribution of each feature to the predicted value. Despite the model's complexity and intricate interactions, the SHAP explanation proved valuable in enhancing the reliability of the predicted results (4).

As the first study (to our knowledge) performed with a habitat and peritumoral signature in survival estimation for patients with early-stage NSCLC, our study demonstrated that the combined nomogram achieved superior prognostic performance than either the single radiomics model or the clinical model alone, with a positive net reclassification improvement. However, several limitations exist in our study. Firstly, the study was retrospective and may be subject to selection bias; therefore, further validation through prospective studies is needed to confirm the clinical applicability of these models. Secondly, since our study did not delineate CT images, multiple models need to be developed. Thirdly, considering that textural features of PET images are significantly influenced by the acquisition and reconstruction methods, variations in scanners could impact the robustness of our model's textural feature analysis. To this end, the sample size of the study was small, and more prospective larger samples and multicenter studies are warranted for further validation.

CONCLUSIONS

In conclusion, an effective radiomics signature was constructed to predict the postoperative survival risk for a specific patient group with pure-solid clinical stage IA non-small cell lung cancer. The radiomics nomogram presented in this study effectively highlights the added value of incorporating the radiomics signature alongside clinical risk factors for personalized PFS estimation. This tool shows promise in guiding individualized postoperative care for patients, though further external validation is needed before it can be widely adopted in clinical practice.

ETHICAL APPROVAL AND CONSENT TO PARTICIPATE

The ethics was approved two hospitals, and waived the need for informed consent due to the retrospective nature of this study.

DECLARATION OF COMPETING INTEREST

The authors declare that they have no known competing financial interests or personal relationships that could have appeared to influence the work reported in this paper.

ACKNOWLEDGMENTS

Not applicable.

AUTHOR CONTRIBUTIONS

B.H.X., K.T., and L.X.W. contributed to the conception or design of the work. S.L.C., J.P.L., and X.W.Z. contributed to the acquisition and analysis of data for the work. L.L.W., J.G.X., and X.W.Z. are responsible for the interpretation of data. B.H.X. and S.L.C. drafted the manuscript. K.T. and L.X.W. critically revised the manuscript. All authors read and approved the final manuscript.

CONSENT FOR PUBLICATION

Not applicable.

STATISTICS AND BIOMETRY

No complex statistical methods were necessary for this paper.

REFERENCES

1. Siegel RL, Miller KD, Wagle NS, et al. Cancer statistics, 2023. CA Cancer J Clin 2023; 73(1):17–48.
2. Zhang Y, Vaccarella S, Morgan E, et al. Global variations in lung cancer incidence by histological subtype in 2020: a population-based study. Lancet Oncol 2023; 24(11):1206–1218.
3. Park SB, Kim KU, Park YW, et al. Application of 18 F-fluorodeoxyglucose PET/CT radiomic features and machine learning to predict early recurrence of non-small cell lung cancer after curative-intent therapy. Nucl Med Commun 2023; 44(2):161–168.
4. Yan H, Niimi T, Matsunaga T, et al. Preoperatively predicting survival outcome for clinical stage IA pure-solid non-small cell lung cancer by radiomics-based machine learning. J Thorac Cardiovasc Surg 2025; 169(1):254–266.e9.
5. Hattori A, Suzuki K, Takamochi K, et al. Prognostic impact of a ground-glass opacity component in clinical stage IA non-small cell lung cancer. J Thorac Cardiovasc Surg 2021; 161(4):1469–1480.
6. Hattori A, Matsunaga T, Fukui M, et al. Prognostic impact of very small ground-glass opacity component in stage IA solid predominant non-small cell lung cancer. Semin Thorac Cardiovasc Surg 2024; 36(2):251–260.
7. Deng J, Zhao M, Wang T, et al. A modified T categorization for part-solid lesions in Chinese patients with clinical stage I Non-small cell lung cancer. Lung Cancer 2020; 145:33–39.
8. Fu F, Zhang Y, Wen Z, et al. Distinct prognostic factors in patients with stage I non-small cell lung cancer with radiologic part-solid or solid lesions. J Thorac Oncol Offl Publ Int Assoc Study Lung Cancer 2019; 14(12):2133–2142.
9. Zhang JX, Song W, Chen ZH, et al. Prognostic and predictive value of a microRNA signature in stage II colon cancer: a microRNA expression analysis. Lancet Oncol 2013; 14(13):1295–1306.
10. Wang R, Zhang G, Zhu X, et al. Prognostic implications of LRP1B and its relationship with the tumor-infiltrating immune cells in gastric cancer. Cancers 2023; 15(24):5759.
11. Gillies RJ, Kinahan PE, Hricak H. Radiomics: images are more than pictures, they are data. Radiology 2016; 278(2):563–577.
12. Zhang X, Su GH, Chen Y, et al. Decoding intratumoral heterogeneity: clinical potential of habitat imaging based on radiomics. Radiology 2023; 309(3):e232047.
13. Huang H, Chen H, Zheng D, et al. Habitat-based radiomics analysis for evaluating immediate response in colorectal cancer lung metastases treated by radiofrequency ablation. Cancer Imaging Offl Publ Int Cancer Imaging Soc 2024; 24(1):44.

14. Valiente Fernández M, Lesmes González de Aledo A, Delgado Moya FP, et al. SHAP model explainability in ECMO-PAL mortality prediction: a critical analysis. Intensive Care Med 2023; 49(12):1559.
15. Crombé A, Kataoka M. Breast cancer molecular subtype prediction: Improving interpretability of complex machine-learning models based on multiparametric-MRI features using SHapley Additive exPlanations (SHAP) methodology. Diagnostic Interv Imaging 2024; 105(5):161–162.
16. Camp RL, Dolled-Filhart M, Rimm DL. X-tile: a new bio-informatics tool for biomarker assessment and outcome-based cut-point optimization. Clin Cancer Res Offl J Am Assoc Cancer Res 2004; 10(21):7252–7259.
17. Mu W, Jiang L, Shi Y, et al. Non-invasive measurement of PD-L1 status and prediction of immunotherapy response using deep learning of PET/CT images. J Immunother Cancer 2021; 9(6):e002118.
18. Nioche C, Orlhac F, Boughdad S, et al. LIFEx: a freeware for radiomic feature calculation in multimodality imaging to accelerate advances in the characterization of tumor heterogeneity. Cancer Res 2018; 78(16):4786–4789.
19. Talkhi N, Nooghabi MJ, Esmaily H, et al. Prediction of serum anti-HSP27 antibody titers changes using a light gradient boosting machine (LightGBM) technique. Sci Rep 2023; 13(1):12775.
20. Sujit SJ, Aminu M, Karpinets TV, et al. Enhancing NSCLC recurrence prediction with PET/CT habitat imaging, ctDNA, and integrative radiogenomics-blood insights. Nat Commun 2024; 15(1):3152.
21. Yang M, Li X, Cai C, et al. [(18)F]FDG PET-CT radiomics signature to predict pathological complete response to neoadjuvant chemoimmunotherapy in non-small cell lung cancer: a multicenter study. Eur Radiol 2024; 34(7):4352–4363.
22. Hattori A, Matsunaga T, Takamochi K, et al. Indications for sublobar resection of clinical stage IA radiologic pure-solid lung adenocarcinoma. J Thorac Cardiovasc Surg 2017; 154(3):1100–1108.
23. Chang R, Qi S, Wu Y, et al. Nomograms integrating CT radiomic and deep learning signatures to predict overall survival and progression-free survival in NSCLC patients treated with chemotherapy. Cancer Imaging Offl Publ Int Cancer Imaging Soc 2023; 23(1):101.
24. Pérez-Morales J, Tunali I, Stringfield O, et al. Peritumoral and intratumoral radiomic features predict survival outcomes among patients diagnosed in lung cancer screening. Sci Rep 2020; 10(1):10528.
25. Hattori A, Matsunaga T, Fukui M, et al. Oncological characteristics of epidermal growth factor receptor-mutated clinical stage IA lung adenocarcinoma with radiologically pure-solid appearance. J Thorac Cardiovasc Surg 2023; 168(3):685–696.e2.
26. Zhang Y, Chen J, Yang C, et al. Preoperative prediction of microvascular invasion in hepatocellular carcinoma using diffusion-weighted imaging-based habitat imaging. Eur Radiol 2024; 34(5):3215–3225.
27. Wu J, Meng H, Zhou L, et al. Habitat radiomics and deep learning fusion nomogram to predict EGFR mutation status in stage I non-small cell lung cancer: a multicenter study. Sci Rep 2024; 14(1):15877.
28. Chen Q, Shao J, Xue T, et al. Intratumoral and peritumoral radiomics nomograms for the preoperative prediction of lymphovascular invasion and overall survival in non-small cell lung cancer. Eur Radiol 2023; 33(2):947–958.
29. Wang Y, Lyu D, Hu L, et al. CT-Based Intratumoral and peritumoral radiomics nomograms for the preoperative prediction of spread through air spaces in clinical stage IA non-small cell lung cancer. J Imaging Inf Med 2024; 37(2):520–535.
30. Shang Y, Zeng Y, Luo S, et al. Habitat imaging with tumoral and peritumoral radiomics for prediction of lung adenocarcinoma invasiveness on preoperative chest CT: a multicenter study. AJR Am J Roentgenol 2024.
31. Watanabe Y, Hattori A, Nojiri S, et al. Clinical impact of a small component of ground-glass opacity in solid-dominant clinical stage IA non-small cell lung cancer. J Thorac Cardiovasc Surg 2022; 163(3): 791–801. .e4.
32. Li Z, Xu W, Gu T, et al. Tumor size, but not consolidation-to-tumor ratio, is an independent prognostic factor for part-solid clinical T1 non-small cell lung cancer. Thorac Cancer 2023; 14(6):602–611.
33. Li R, Li Z, Yang Z, et al. The presence of micropapillary and/or solid subtypes is an independent prognostic factor for patients undergoing curative resection for stage I lung adenocarcinoma with ground-glass opacity. Transl Lung Cancer Res 2024; 13(2):256–268.
34. Fan Z, Jiang J, Xiao C, et al. Construction and validation of prognostic models in critically Ill patients with sepsis-associated acute kidney injury: interpretable machine learning approach. J Transl Med 2023; 21(1):406.
35. Takeda A, Yokosuka N, Ohashi T, et al. The maximum standardized uptake value (SUVmax) on FDG-PET is a strong predictor of local recurrence for localized non-small-cell lung cancer after stereotactic body radiotherapy (SBRT). Radiother Oncol J Eur Soc Ther Radiol Oncol 2011; 101(2):291–297.
36. Tapias LF, Shen R, Cassivi SD, et al. Impact of FDG PET standardized uptake value in resected clinical stage IA non-small cell lung cancer. Ann Thorac Surg 2024; 117(5):1017–1023.